Calculation of Force Excitations in Induction Machines With Centric and Excentric Positioned Rotor Using 2-D Transient FEM

Christoph Schlensok and Gerhard Henneberger

***Abstract*—The calculation of induction machines with squirrel cages using the finite-element method (FEM) requires a transient solving process. The rotation has to be taken into account. Therefore, a rotating air gap is implemented. The formulation for the transient solver is given. Finite-element models of an induction machine with centrical and excentrical positioned rotor are calculated. The formulation for the computation of the surface force density on the stator teeth is presented. For both variants of the induction machine, the forces are calculated and compared.**

***Index Terms*—Excentricity, induction machine with squirrel cage, surface force density, transient 2-D FEM calculation.**

I. Introduction

DUE to fabrication tolerances, the rotors of electrical machines are usually not positioned centrically. In case of an induction machine used as a power-steering drive, this affects the acoustic behavior and, therefore, the customer satisfaction. In order to estimate the effect of excentricity, the force density on the stator teeth has to be calculated. In this paper, two variants of an induction machine with squirrel cage are compared. The rotor of the first variant is positioned centrically. In case of the second variant, the rotor is shifted radially but is still rotating around the stator axis. This kind of excentricity is called dynamic excentricity. Both variants are calculated with a two–dimensional (2-D)-transient solver, and afterwards, the force excitations on the stator teeth are computed.

II. Formulation of the Transient Solver

The applied solver is part of an object-oriented solver package [1]. The transient FEM formulation takes the rotational movement into account, and two finite-element meshes have to be handled. The 2-D $\vec{A}$-approach is node based. The magnetic vector potential is used in all regions. The equation

$$\int_\Gamma (\nabla \cdot \alpha_i \cdot \nu \cdot \nabla \cdot A_z(t) + \alpha_i \cdot \sigma \cdot \frac{\partial}{\partial t} A_z(t)) \mathrm{d}\Gamma = \int_\Gamma (\alpha_i \cdot J_{z0}(t)) \, \mathrm{d}\Gamma \quad (1)$$

has to be solved in the complete model Γ and is given in Galerkin formulation [2]. The material parameters ν and σ represent the nonlinear reluctivity and the linear conductivity. The shape function of an element is defined by α_i. Triangular-shaped elements are used. $J_{z0}(t)$ describes the z-component of the given coil current-density as the only excitation.

For linear interpolation of the time-dependent variables, the first order time-step algorithm is applied, and $A(t)$ can be written as a function of time:

$$A(t) = (1 - \Theta) A_n + \Theta A_{n+1} \quad (2)$$

$$\Theta = \frac{t - t_n}{t_{n+1} - t_n} = \frac{t - t_n}{\Delta t}; \qquad 0 \le \Theta \le 1. \quad (3)$$

Θ is the weighting parameter and set to $\Theta = (2/3)$ according to the Galerkin scheme [3].

III. Formulation for the Calculation of the Surface Force Density

With the Maxwell stress tensor

$$\vec{\sigma} = \frac{1}{2} \vec{n}_{12} [B_n (H_{1n} - H_{2n}) - (w_1' - w_2')] \quad (4)$$

an expression for the local surface force density is given [4]. The index n stands for the normal components of the vectors $\vec{B}$ and $\vec{H}$. $\vec{n}_{12}$ is the normal vector of the boundary surface from region 2 to 1. w_1' and w_2' are the magnetic-coenergy densities of these regions.

IV. Finite-Element Models

For the regarded application, investigations have shown that an induction machine with $N_S = 24$ stator slots and $N_R = 26$ rotor bars provides a very good variant [5]. The lamination is shown in Fig. 1. Although only two pole pitches are depicted, the machine is modeled as a 360°-model since the number of elements is small for 2-D calculation in general. The models have about 25 000 first-order triangular elements and 12 500 nodes.

In Fig. 2, closeups of the air gaps of the centrical and the excentrical model are opposed. To the left, the centrical model is depicted. The air gap has a constant value of $\delta = 0.3$ mm. Next to it, the excentrical model is shown. The air gap differs between $\delta_{\min} = 0.2$ and $\delta_{\max} = 0.4$ mm. The maximum air gap is depicted. In both cases, the air gap has three layers of elements in order to increase the exactness of the torque and force calculation. This way, the nodes of the layer in the middle that is sliced are assigned to one material only.

Manuscript received July 1, 2003.

The authors are with the Department of Electrical Machines (IEM), Aachen University (RWTH), D-52056 Aachen, Germany (e-mail: christoph.schlensok@iem.rwth-aachen.de).

Digital Object Identifier 10.1109/TMAG.2004.825468

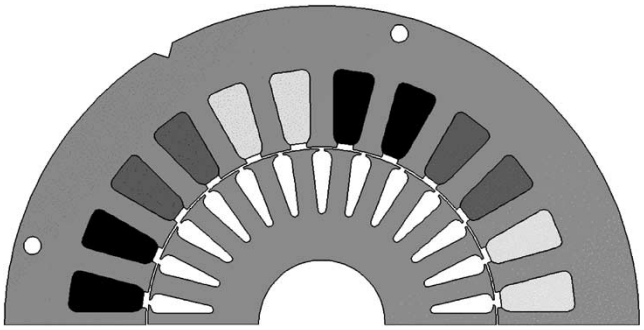

Fig. 1. Lamination of the induction machine—two pole pitches.

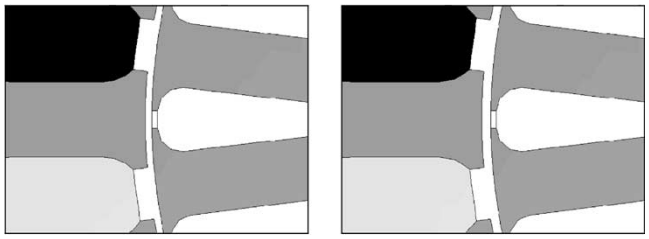

Fig. 2. Closeups of air gap in centrical and excentrical model.

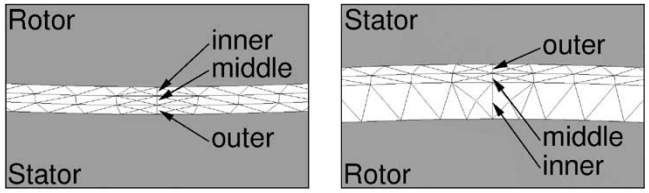

Fig. 3. Meshed excentrical air gap for excentrical model.

The rotating air gap requires circular revolution. In case of the centrically positioned rotor, all three layers are formed circularly, but if the rotor is shifted into an excentrical position, the air gap is asymmetrical and needs extra treatment. For both models, the outer air-gap layer is connected to the stator and the inner to the rotor. The middle layer is remeshed in each time step. In order to keep good quality element shapes, the middle layer is modeled as annulus again. In turn, this means that the inner layer cannot be an annulus any longer. Hence, the outer layer is circular. Fig. 3 shows this effect for the meshed model on the narrow [Fig. 3(a)] and the wide [Fig. 3(b)] side of the excentrical air gap. The layers are modeled equidistantly on the narrow side.

V. Two-Dimensional Transient FEM Calculation

In a first step, the two variants are calculated with the 2-D transient solver. The point of operation is at $n = 1200$ min^{-1} with $f_1 = 50.2$ Hz. The sinusoidal stator current densities are sampled with 64 steps per period. The resulting time step is $\Delta t = 311\ \mu$s. The torque, of which the time-dependent behavior is depicted in Fig. 4(a), and the overall force are computed.

The average torque is not affected strongly by the excentricity, as Table I shows [6], but for the overall forces, the excentricity has very strong effect, as listed in Table I. The reason

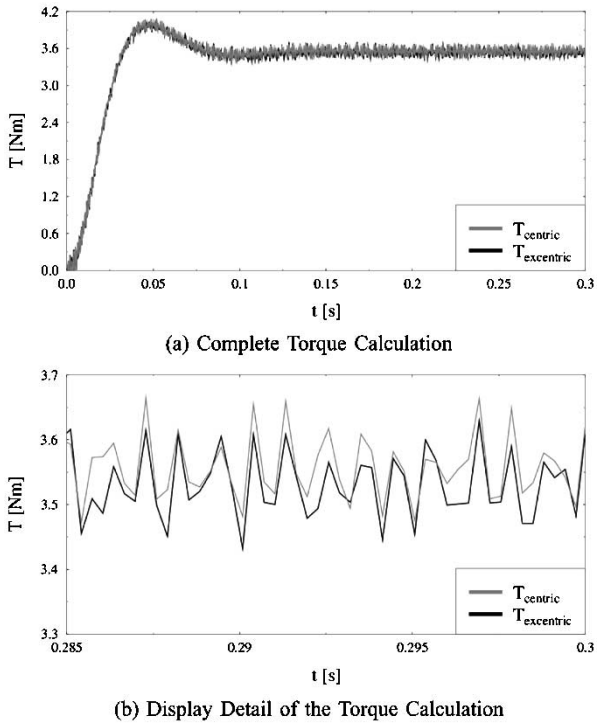

Fig. 4. Time-dependent torque behavior.

TABLE I
Torque and Force: Average Values and Maximum Ripple

	$\overline{T}$ [Nm]	ΔT [Nm]
Centrical Case	3.555	0.252
Excentrical Case	3.535	0.301
	$\overline{F}$ [N]	ΔF [N]
Centrical Case	0.012	0.156
Excentrical Case	98.957	51.569

is rather trivial. The normal component of the electromagnetic force between rotor and stator is much higher than the tangential and axial components. If the rotor is positioned excentrically, the radial force on the one side of the rotor is not compensated completely on the opposite side. The force increases depending on the extent of excentricity.

In Fig. 5, the force behavior of the absolute value F and the components F_x and F_y for the excentrical machine model are depicted. The absolute value of the global force pulsates strongly [Fig. 5(a)]. If the two components are regarded, the revolution of the global force for dynamic excentricity can be seen [7]. The x- and y-component are sinusoidal and have a phase shift of $\beta = 90°$.

The time-dependent force behaviors for both variants are analyzed using the fast Fourier transformation (FFT). The results are depicted in Fig. 6. Since the global force is very small in case of the centrically positioned rotor, there is no reasonable analysis possible in the spectrum. For the excentrical case, the stronger excitation has a strong effect on the spectrum as well. Next to the average value of the global force at $f = 0$ Hz, there are some further significant orders detected. These are located at $f = 301$, 460, 480, 760, 942, 1242, and 1512 Hz. The rotor

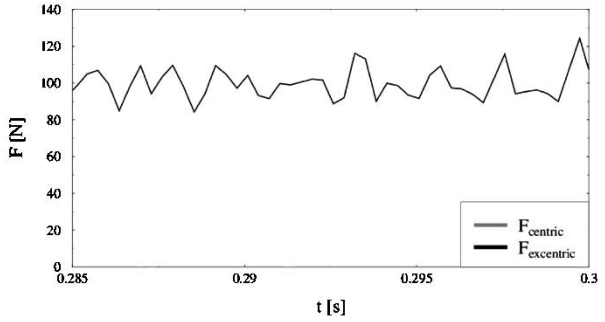

(a) Behaviour of Absolute Value of Global Force

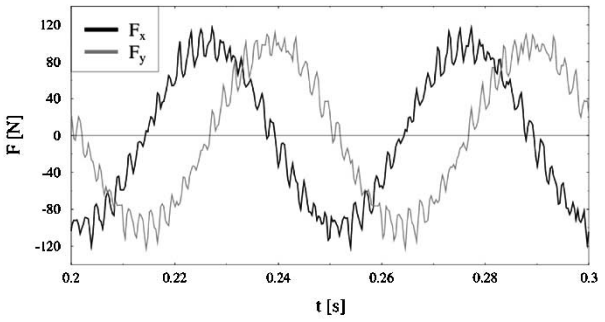

(b) Components F_x and F_y of the Global Force

Fig. 5. Behavior of the global force in excentrical case.

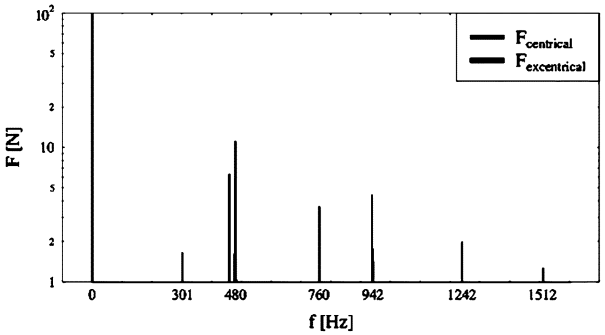

Fig. 6. Spectrum of the global force.

speed $f = 20$ Hz is not found in the global force because of the geometrically averaging of the x- and y-components.

VI. Surface Force Density Calculation

In a next step, (4) is used to calculate the surface force density on the stator teeth. The force density is only computed toward the air gap since the forces between the lamination and the copper winding are much smaller. The main excitation will appear in radial direction toward the rotor. Usually, the normal forces are about 10 to 100 times or even more than the tangential ones, as described in Section V before.

Fig. 7 shows the surface force density-distribution for the same time step for both variants. In case of the centrical variant, the forces that occur on the one side of the stator are compensated on the opposite side. If compared with the force excitation for the excentrical case, the forces no longer have the same value on the opposite sides. Consequently, they are not compensated. The stator teeth are excited asymmetrically with the rotor speed and higher orders of this.

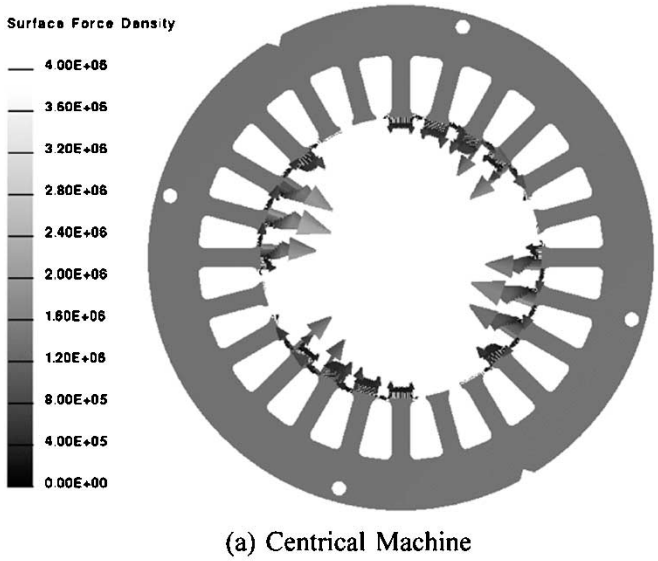

(a) Centrical Machine

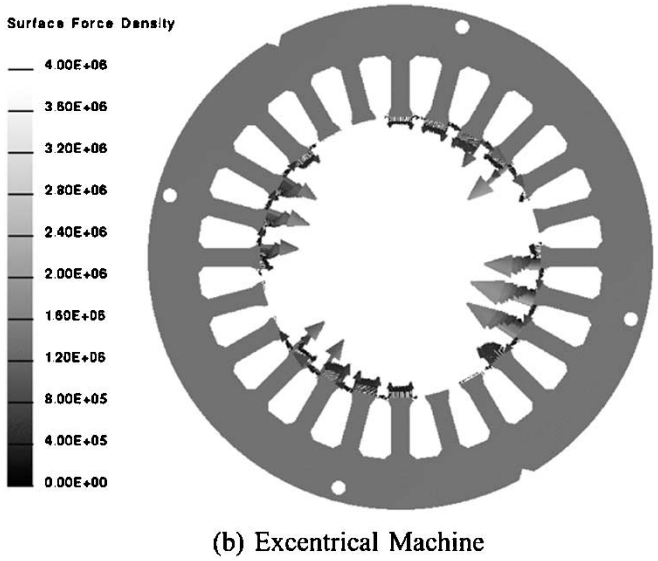

(b) Excentrical Machine

Fig. 7. Surface force densities for both variants at same time step.

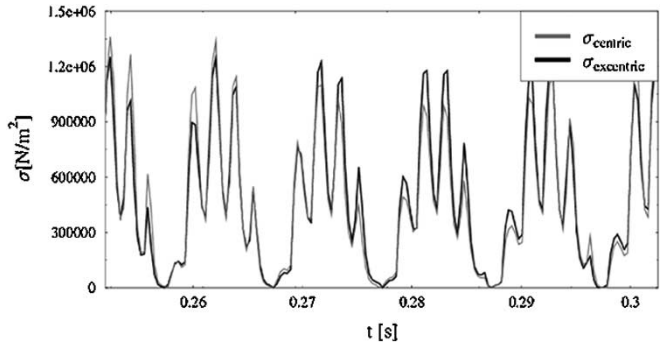

Fig. 8. Behavior of force density at one stator tooth element.

Fig. 8 shows the force excitation along the edge of one stator tooth for both cases. The force density behaves similarly for both variants. The maximum excitation reaches the same level and is nearly the same for each ripple stemming from the slotting of the rotor. Therefore, there is no significant difference for the surface force-density excitation when the rotor is positioned excentrically.

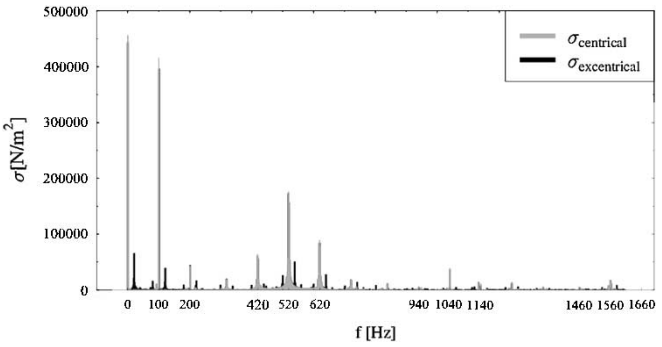

Fig. 9. Spectrums of force density at one stator tooth element.

TABLE II
ORDERS AND VALUES OF SURFACE FORCE-DENSITY ($f_1 = 50.2$ Hz STATOR FREQUENCY, $f_R = 20$ Hz ROTOR SPEED)

	f [Hz]	$\sigma_{centrical}$ [$\frac{\mathrm{N}}{\mathrm{m}^2}$]	$\sigma_{excentrical}$ [$\frac{\mathrm{N}}{\mathrm{m}^2}$]
f_R	20.0	780	65970
$2 \cdot f_1$	100.4	415341	396519
$21 \cdot f_R$	419.6	63455	60819
$26 \cdot f_R$	520.0	176495	173016
$31 \cdot f_R$	620.4	89195	84141
$47 \cdot f_R$	939.6	6734	4639
$52 \cdot f_R$	1040.0	38776	36268
$57 \cdot f_R$	1140.4	11135	7832

Finally, the surface force density is analyzed using the FFT. Fig. 9 shows the results for both variants. The significant frequencies are others than those of the global force in Fig. 6. The order of the force density and their values are listed in Table II. The values for all detected orders, except for the first order of the rotor speed, do not differ significantly, depending on the variant. The orders found are next to twice the stator frequency, the rotor-slot harmonics (26., 52., and 78.), and their modulation with five times the stator frequency (21., 31., 47., and higher). The only main difference between the excitation of the centrical and the excentrical variant is the first order of the rotor speed at $f_R = 20$ Hz. The revolving force excitation found in Fig. 5(b) is reflected here. The other orders enumerated above are also modulated with f_R in the case of the excentrical rotor, as Fig. 9 shows. The orders found in the force-density excitation fit those of structure-borne sound measurements made by the project partner in industry, with the exception of the higher orders of the stator frequency. Acoustic calculations have shown that these are indeed negligible.

VII. CONCLUSION

In this paper, an induction machine with squirrel cage as power-steering drive is calculated with a 2-D transient solver. The machine geometry is varied by placing the rotor centrically and excentrically. The torque and the overall force on the rotor are computed and compared. Although the average torque and its behavior are not significantly affected by the excentricity, the overall forces rise strongly.

The surface force density on the stator teeth is calculated for both variants. The excentricity has strong effect on the surface force density distribution. The forces on the one side of the machine are no longer compensated on the other side. The stator teeth are excited asymmetrically. This results in joggling forces, which will generate extra noise.

The surface force density and the global force are analyzed using the FFT. The orders found in the spectrum of the global force do not match those of the surface force density, which is reasonable since the overall force is a global value calculated in the air gap and the surface force density a local value computed for one stator tooth element. For both variants, the surface force density shows the same significant orders plus some extra ones in case of excentricity. The stator teeth are excited with twice the stator frequency, with the first rotor slot harmonic, its modulation with twice the stator frequency, and with multiples of these orders. In case of excentricity, the teeth are also excited with rotor speed, and the orders mentioned before are modulated with rotor speed as well.

Structure-borne sound measurements have shown that the orders found in the analysis of the surface force density are responsible for the noise caused by the induction machine. Dynamical excentricity generates extra excitation and is responsible for joggling forces. It is not as critical as expected.

REFERENCES

[1] G. Arians, T. Bauer, C. Kaehler, W. Mai, C. Monzel, D. van Riesen, and C. Schlensok, "Innovative modern object-oriented solving environment — iMOOSE,", Aachen, Germany, http://www.imoose.de.

[2] G. Arians and G. Henneberger, "Object oriented analysis and design of transient finite element solvers applied to coupled problems," in *Proc. 9th Conf. Electromagn. Field Comput.*, WI, 2000.

[3] O. C. Zienkiewicz and R. L. Taylor, *The Finite Element Method*. London, U.K.: McGraw-Hill, 1989, pp. 346–361.

[4] I. Ramesohl, S. Küppers, W. Hadrys, and G. Henneberger, "Three dimensional calculation of magnetic forces and displacements of a claw-pole generator," *IEEE Trans. Magn.*, vol. 32, pp. 1685–1688, May 1996.

[5] C. Schlensok and G. Henneberger, "Torque behavior in induction machines due to skewing," in *Proc. 3rd Int. Seminar Vibrations Acoustic NoiseElectric Machinery*, Łóodź, Poland, Oct. 2002.

[6] J. Rusek, "Effect of static plus dynamic eccentricity on static and dynamic behavior of induction machines," in *Proc. 3rd Int. Seminar Vibrations Acoust. Noise Electric Machinery*, Łóodź, Poland, Oct. 2002.

[7] C. Schlensok and G. Henneberger, "Comparison of static, dynamic and static-dynamic excentricity in induction machines with squirrel cages using 2D-transient FEM," in *Proc. 6th Int. Symp. Electr. Magn. Fields*, Aachen, Germany, Oct. 2003.